Electronic Supplementary Material (ESI) for Journal of Materials Chemistry C.

Supplementary Information

Photoinduced effects on the magnetic properties of the $(Fe_{0.2}Cr_{0.8})_{1.5}[Cr(CN)_6]$ Prussian blue analogue.†

Francisco Jesús Luque,[a] Iwona Agnieszka Kowalik,[b] Juan Pablo Prieto-Ruiz,[c] Miguel Ángel Niño,[d] Helena Prima-García,[c] Francisco Manuel Romero,[c] Dimitri Arvanitis,[e] Corine Mathonière,[f,g] Eugenio Coronado,[c] Rodolfo Miranda,[a,d,h] and Juan José de Miguel*[a,h,i]

Sample preparation

The $(Fe_{0.2}Cr_{0.8})_{1.5}[Cr(CN)_6]\cdot 15\ H_2O$ Prussian blue analogue (PBA) films used in this work were fabricated by electrodeposition onto 5×10 mm^2 Mylar substrates covered by an evaporated, 100 nm-thick Au film. The electrochemical cell was charged with a 20 mL aqueous solution containing $K_3[Cr(CN)_6]$ (5 mM), $CrCl_3$ (6.7 mM) and $FeCl_3$ (1.1 mM) as reported in the literature.[1,2] The chemicals were purchased from Sigma-Aldrich and used without further purification. The deposition was carried out at a fixed potential of -0.8 V. A commercial Ag/AgCl (3M NaCl) reference electrode and a Pt counter electrode were also employed. The deposition process was controlled by a Metrohm AUTOLAB potentiostat operating in coulometry mode. After growth the films were rinsed with mili-Q water and dried at room temperature. Since the thickness of electrodeposited $Cr_{5.5}(CN)_{12}\cdot 11.5\ H_2O$ films was found to increase linearly with deposition time in a previous study,[3] this parameter has been used to control the thicknesses of the samples prepared for this work. The thin films used for the XAS measurements were obtained using a short electrodeposition pulse of 5 seconds; the thicker EXAFS samples required 100 seconds of deposition. The films' thicknesses were cross-checked after growth by means of an Ambios Technology XP-1 profilometer. Further compositional and morphological characterisation has been presented in our previous publication.[4]

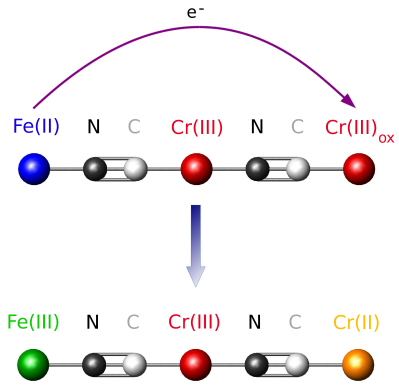

Fig. S.1 Schematic representation of the model with 3 metal centres proposed in the text and the charge transfer process from Fe^{II} to Cr^{III}_{ox} across the bridging Cr^{III}.

[a] Departamento de Física de la Materia Condensada, Universidad Autónoma de Madrid, Cantoblanco, 28049-Madrid, Spain.
[b] Institute of Physics, Polish Academy of Sciences, 02668-Warsaw, Poland.
[c] Instituto de Ciencia Molecular (ICMol), Universitat de València, 46980-Paterna, Spain.
[d] IMDEA-Nanoscience, Cantoblanco, 28049 Madrid, Spain.
[e] Department of Physics and Astronomy, Uppsala University, 75237-Uppsala, Sweden.
[f] CNRS, ICMCB, UPR 9048, F-33800 Pessac, France.
[g] Univ. Bordeaux, ICMCB, UPR 9048, F-33700 Pessac, France.
[h] Condensed Matter Physics Center (IFIMAC), Universidad Autónoma de Madrid, Cantoblanco, 28049 Madrid, Spain.
[i] Instituto de Física de Materiales "Nicolás Cabrera", Universidad Autónoma de Madrid, Cantoblanco, 28049 Madrid, Spain. E-mail: juanjose.demiguel@uam.es

Ligand Field parameters

The whole sets of parameters used to analyse the XAS spectra discussed in the manuscript are listed in the following tables. The fits to the data have been carried out with the CTM4XAS package,[6,7] which is based on the TT-Multiplet code of Thole and Ogasawara.[8,9] For those not familiar with this software, the physical meaning of these parameters can be briefly described as follows:

- *Atomic multiplet parameters:*
  - κ, the Slater-Condon parameter or percentage of reduction of the Slater integrals. Measures the covalency of the interaction between the metal and the ligand, with low values of κ corresponding to covalent bonds.
  - ζ_{2p}, the magnitude of the spin-orbit coupling (SOC) for the $2p$ orbitals. This parameter controls the energy separation between the L_2 and L_3 edges.
  - ζ_{3d}, SOC for the $3d$ orbitals. Although weak (of the order of 10^{-2} eV), it can have significant effects because it controls whether Hund's third rule is applicable or not in the ground state.
- *Crystal field parameters:* The crystal field splitting $10Dq$ represents the splitting between the e_g and t_{2g} subbands in octahedral symmetry. When the symmetry is reduced, these levels can be split further, with energy separations controlled by the parameters D_t and D_s.
- *Charge transfer parameters:* The hybridization between the metal centre and the surrounding ligands is accounted for by considering the interaction between two or more electronic configurations.
  - EG (EF) gives the difference in energy of both configurations in the ground (excited) state.
  - In octahedral symmetry, the hopping integrals T_{e_g} and $T_{t_{2g}}$ control the mixing of the electronic states of the different configurations, giving rise to the formation of σ or π-type bonds, respectively.
  - If the symmetry is reduced the hopping integrals are denoted T_{b_1}, T_{a_1}, T_{b_2}, and T_e.

Table S.I Set of Ligand Field parameters for Fe^{II} HS used with the CTM4XAS[7] software package to fit the experimental XAS spectra.

		300 K	300 K green light	150 K	150 K green light
	κ (%)	100	100	100	100
	ζ_{2p} (eV)	7.79	7.79	7.79	7.79
	ζ_{3d} (eV)	0.000	0.000	0.000	0.000
	$10Dq$ (eV)	0.8	0.7	0.9	0.8
	D_t (eV)	0.040	0.040	0.025	0.050
	D_s (eV)	0.070	−0.030	0.012	0.050
LMCT	$EG2$	0.0	0.0	0.0	0.0
	$EF2$	0.0	0.0	0.0	0.0
	T_{b_1}	0.0	0.0	0.0	0.0
	T_{a_1}	0.0	0.0	0.0	0.0
	T_{b_2}	0.0	0.0	0.0	0.0
	T_e	0.0	0.0	0.0	0.0
MLCT	$EG2$	1.5	1.2	1.7	1.5
	$EF2$	0.5	0.2	0.8	0.5
	T_{b_1}	2.8	2.9	3.1	2.8
	T_{a_1}	2.5	2.9	3.1	2.5
	T_{b_2}	3.8	3.5	3.4	3.8
	T_e	3.4	3.5	3.5	3.4
Configuration	% $\lvert 3d^5\mathrm{L}^-\rangle$	48	48	47	48
	% $\lvert 3d^6\rangle$	52	52	53	52
	% $\lvert 3d^7\underline{\mathrm{L}}\rangle$	0	0	0	0
# holes		4.48	4.48	4.47	4.48

Table S.II Set of Ligand Field parameters for Fe^{II} LS.

		300 K	300 K green light	150 K	150 K green light
	κ (%)	50	—	50	50
	ζ_{2p} (eV)	8.20	—	8.20	8.20
	ζ_{3d} (eV)	0.067	—	0.067	0.067
	$10Dq$ (eV)	2.3	—	2.5	2.2
	D_t (eV)	0.000	—	0.000	0.000
	D_s (eV)	0.000	—	0.000	0.000
LMCT	$EG2$	3.0	—	2.3	3.5
	$EF2$	2.0	—	1.3	2.5
	T_{b_1}	1.1	—	1.1	1.1
	T_{a_1}	1.1	—	1.1	1.1
	T_{b_2}	1.8	—	1.8	1.8
	T_e	1.8	—	1.8	1.8
MLCT	$EG2$	0.0	—	0.0	0.0
	$EF2$	0.0	—	0.0	0.0
	T_{b_1}	0.0	—	0.0	0.0
	T_{a_1}	0.0	—	0.0	0.0
	T_{b_2}	0.0	—	0.0	0.0
	T_e	0.0	—	0.0	0.0
Configuration	% $\lvert 3d^5\mathrm{L}^-\rangle$	30	—	33	28
	% $\lvert 3d^6\rangle$	70	—	67	72
	% $\lvert 3d^7\underline{\mathrm{L}}\rangle$	0	—	0	0
# holes		4.30	—	4.33	4.28

Table S.III Ligand Field parameters for Fe^{III}.

		300 K	300 K green light	150 K	150 K green light
	κ (%)	80	80	80	80
	ζ_{2p} (eV)	7.79	7.79	7.79	7.79
	ζ_{3d} (eV)	0.064	0.064	0.064	0.064
	$10Dq$ (eV)	1.1	1.1	1.3	1.2
	D_t (eV)	0.000	0.000	0.000	0.000
	D_s (eV)	0.000	0.000	0.000	0.000
LMCT	$EG2$	0.9	0.5	0.5	0.5
	$EF2$	0.0	0.0	0.0	0.0
	T_{b_1}	0.8	0.8	0.8	0.8
	T_{a_1}	0.8	0.8	0.8	0.8
	T_{b_2}	1.0	1.0	1.0	1.0
	T_e	1.0	1.0	1.0	1.0
MLCT	$EG3$	0.9	1.7	0.9	0.8
	$EF3$	2.5	3.2	2.5	2.4
	T_{b_1}	1.7	1.7	1.6	1.7
	T_{a_1}	1.7	1.7	1.6	1.7
	T_{b_2}	0.6	0.6	0.7	0.7
	T_e	0.6	0.6	0.7	0.7
Configuration	% $\lvert 3d^4\mathrm{L}^-\rangle$	29	22	25	28
	% $\lvert 3d^5\rangle$	56	62	60	59
	% $\lvert 3d^6\underline{\mathrm{L}}\rangle$	15	16	15	13
# holes		5.15	5.07	5.10	5.14

Table S.IV Ligand Field parameters for Cr^{II} HS.

		300 K	300 K green light	150 K	150 K green light
	κ (%)	80	80	80	80
	ζ_{2p} (eV)	5.78	5.78	5.78	5.78
	ζ_{3d} (eV)	0.042	0.042	0.042	0.042
	$10Dq$ (eV)	0.7	0.7	1.1	0.8
	D_t (eV)	0.020	0.020	0.100	0.040
	D_s (eV)	−0.140	−0.140	−0.050	−0.140
LMCT	$EG3$	6.0	5.5	2.5	5.5
	$EF3$	6.5	6.5	3.0	6.5
	T_{b_1}	1.4	1.4	1.2	1.6
	T_{a_1}	1.4	1.4	1.2	1.6
	T_{b_2}	0.7	0.7	0.6	0.8
	T_e	0.7	0.7	0.6	0.8
MLCT	$EG2$	−0.6	−1.1	−2.1	−0.5
	$EF2$	−2.6	−3.0	−4.1	−2.5
	T_{b_1}	1.6	1.5	1.1	1.1
	T_{a_1}	1.6	1.5	1.9	1.5
	T_{b_2}	0.4	0.4	0.5	0.4
	T_e	0.4	0.4	0.5	0.4
Configuration	% $\lvert 3d^3\mathrm{L}^-\rangle$	24	18	17	21
	% $\lvert 3d^4\rangle$	70	75	75	70
	% $\lvert 3d^5\underline{\mathrm{L}}\rangle$	6	7	8	9
# holes		6.18	6.12	6.08	6.13

Table S.V Ligand Field parameters for Cr^{III}.

		300 K	300 K green light	150 K	150 K green light
	κ (%)	70	70	80	70
	ζ_{2p} (eV)	5.78	5.78	5.78	5.78
	ζ_{3d} (eV)	0.000	0.000	0.000	0.048
	$10Dq$ (eV)	2.7	2.8	2.4	2.6
	D_t (eV)	−0.020	−0.020	−0.060	−0.040
	D_s (eV)	0.120	0.140	0.120	0.100
LMCT	$EG2$	−4.2	−4.2	−4.3	−4.2
	$EF2$	−6.0	−6.0	−6.0	−6.0
	T_{b_1}	0.5	0.5	0.5	0.5
	T_{a_1}	0.5	0.5	0.5	0.5
	T_{b_2}	0.2	0.2	0.2	0.2
	T_e	0.2	0.2	0.2	0.2
MLCT	$EG3$	−2.5	−2.5	−2.5	−2.5
	$EF3$	−1.5	−1.5	−1.5	−1.5
	T_{b_1}	0.6	0.7	1.1	0.6
	T_{a_1}	0.6	0.8	1.0	0.7
	T_{b_2}	1.3	1.1	1.8	1.3
	T_e	0.9	0.8	1.6	0.8
Configuration	% $\lvert 3d^2\mathrm{L}^-\rangle$	15	12	22	14
	% $\lvert 3d^3\rangle$	83	86	76	84
	% $\lvert 3d^4\underline{\mathrm{L}}\rangle$	2	2	2	2
# holes		7.13	7.10	7.20	7.12

Table S.VI Ligand Field parameters for Cr^{III} WCF.

		300 K	300 K green light	150 K	150 K green light
	κ (%)	90	—	90	90
	ζ_{2p} (eV)	5.67	—	5.67	5.67
	ζ_{3d} (eV)	0.047	—	0.047	0.047
	$10Dq$ (eV)	1.2	—	1.2	1.2
	D_t (eV)	0.050	—	0.050	0.050
	D_s (eV)	0.020	—	0.020	0.020
LMCT	$EG2$	−0.7	—	−0.7	−0.7
	$EF2$	−2.1	—	−2.1	−2.1
	T_{b_1}	1.5	—	1.5	1.5
	T_{a_1}	1.5	—	1.5	1.5
	T_{b_2}	0.2	—	0.2	0.2
	T_e	0.2	—	0.2	0.2
MLCT	$EG3$	−1.0	—	−1.0	−1.0
	$EF3$	0.0	—	0.0	0.0
	T_{b_1}	0.6	—	0.6	0.6
	T_{a_1}	0.6	—	0.6	0.6
	T_{b_2}	1.4	—	1.4	1.4
	T_e	1.4	—	1.4	1.4
Configuration	% $\lvert 3d^2\mathrm{L}^-\rangle$	12	—	12	12
	% $\lvert 3d^3\rangle$	57	—	57	57
	% $\lvert 3d^4\underline{\mathrm{L}}\rangle$	31	—	31	31
# holes		6.82	—	6.82	6.82

Table S.VII Ligand Field parameters for Cr^{IV}.

		300 K	300 K green light	150 K	150 K green light
	κ (%)	90	90	90	90
	ζ_{2p} (eV)	5.67	5.67	5.67	5.67
	ζ_{3d} (eV)	0.047	0.47	0.047	0.047
	$10Dq$ (eV)	1.1	1.1	1.3	1.1
	D_t (eV)	0.020	0.020	0.150	0.020
	D_s (eV)	−0.020	−0.020	−0.200	−0.015
LMCT	$EG2$	4.0	4.0	4.5	4.0
	$EF2$	3.0	3.0	3.5	3.0
	T_{b_1}	0.0	0.0	0.0	0.0
	T_{a_1}	0.5	0.5	0.8	0.5
	T_{b_2}	1.7	1.7	2.0	1.7
	T_e	1.3	1.3	1.0	1.3
MLCT	$EG3$	0.0	0.0	0.0	0.0
	$EF3$	0.0	0.0	0.0	0.0
	T_{b_1}	0.0	0.0	0.0	0.0
	T_{a_1}	0.0	0.0	0.0	0.0
	T_{b_2}	0.0	0.0	0.0	0.0
	T_e	0.0	0.0	0.0	0.0
Configuration	% $\lvert 3d^1\mathrm{L}^-\rangle$	0	0	0	0
	% $\lvert 3d^2\rangle$	74	74	81	74
	% $\lvert 3d^3\underline{\mathrm{L}}\rangle$	26	26	19	26
# holes		7.74	7.74	7.81	7.74

EXAFS analysis

Table S.VIII summarizes the interatomic distances and unit cell sizes determined from our analysis of the EXAFS measurements.

Table S.VIII Summary of interatomic distances and unit cell sizes derived from the analysis of the EXAFS measurements at 295 K.

Shell	d_N (Å)	d_C (Å)	Unit cell size (Å)
Fe^{II} HS–N≡C–Cr^{III}	$d(Fe^{II}–N)$ = 2.12±0.01	$d(Cr^{III}–C)$ = 2.05±0.01	10.72±0.03
Fe^{II} LS–C≡N–Cr^{III} WCF	$d(Cr^{III}–N)$ = 2.13±0.03	$d(Fe^{II}–C)$ = 2.03±0.04	10.65±0.03
Fe^{III}–N≡C–Cr^{III}	$d(Fe^{III}–N)$ = 2.08±0.04	$d(Cr^{III}–C)$ = 2.04±0.01	10.51±0.01
Cr^{II}–N≡C–Cr^{III}	$d(Cr^{II}–N)$ = 2.11±0.01	$d(Cr^{III}–C)$ = 2.01±0.01	10.55±0.01
Cr^{III}–N≡C–Cr^{III}	$d(Cr^{III}–N)$ = 2.04±0.02	$d(Cr^{III}–C)$ = 2.01±0.02	10.55±0.02

The following tables, S.IX and S.X list the main parameters resulting from the fits to the EXAFS data of Fe and Cr respectively by the Athena and Artemis programmes.[10,11] In brief, the physical meaning of these parameters is the following:

- S_0^2 is a dimensionless factor applied to the EXAFS amplitude to account for many body effects, such as those due to multiple electron excitations.
- E_0 is the threshold energy; it is closely related to the edge energy, but it can be modified during the fitting procedure by an amount ΔE.
- Δr is the change with respect to the initial half-path length, caused by the potential-dependent phase shifts.
- The Debye-Waller factor takes into account the effects of thermal and structural disorder, and is measured in terms of the mean square relative displacements of the neighbouring atoms involved in the scattering process.

Table S.IX Fitting parameters for the EXAFS measurements on Fe (Figure 3 in the paper).

Shell	Path	$S_0^2(k)$	ΔE (eV)	Δr (Å)	Debye-Waller ($Å^2$)
[1] Fe^{II}–N≡C–Cr^{III}	Fe–N	0.73	7.90	-0.0275	0.01185
	Fe–C	1.100225	6.56	-0.039	0.021
	Fe–(N–C)	0.55	5.66	0.0	0.017
	Fe–Cr	1.03729	-2.797531	0.06	0.011093
[2] Fe^{II}–C≡N–Cr^{III}	Fe–C	1.19	-10.0	0.08	0.0007
	Fe–N	0.95372	-10.0	0.039545	0.0028
	Fe–(C–N)	0.90	10.0	0.0	0.00497
	Fe–Cr	1.199887	-9.999987	-0.077298	0.001
[3] Fe^{III}–N≡C–Cr^{III}	Fe–N	0.90	10.0	-0.07	0.0045
	Fe–C	0.90	-1.28	-0.139	0.01027
	Fe–(N–C)	1.0	10.0	0.0	0.0052
	Fe–Cr	1.199741	-0.35046	-0.046	0.004866

Table S.X Fitting parameters for the EXAFS measurements on Cr (Figure 6 in the paper).

Shell	Path	$S_0^2(k)$	ΔE (eV)	Δr (Å)	Debye-Waller (Å^2)
[1] Cr^{III}–C≡N–Fe^{II}	Cr–C	1.1	2.278966	0	0.00308
	Cr–N	1.18199864	9.996927	0	0.000406
	Cr–(C–N)	1.199714	9.997517	0	0.012396
	Cr–Fe	1.199633	-9.993602	0	0.000121
[2] Cr^{III}–N≡C–Fe^{II}	Cr–C	1.1904161	-8.201773	0	0.00203169
	Cr–N	1.000846869	-0.758431	0	0.006439
	Cr–(N–C)	0.9199735	6.040356	0	0.007126
	Cr–Fe	1.199791	-7.97025	0	0.001079
[3] Cr^{III}–C≡N–Fe^{III}	Cr–C	0.7053962	10	0	0.0056
	Cr–N	1.18984	0	0	0.005162
	Cr–(C–N)	1.1992016	0.552939	0	0.017
	Cr–Cr	1.00697	9.885946	0	0.004137
[4] Cr^{III}–C≡N–Cr^{III}	Cr–C	0.85	6.389788	0	0.002831
	Cr–N	1.19	6.327053	0.039142	0.0020439
	Cr–(C–N)	1.18	-4.833741	0	0.007227
	Cr–Cr	1.15	-9.989881	-0.024962	0.002093
[5] Cr^{III}–N≡C–Cr^{III}	Cr–C	1.05	10	0	0.004821
	Cr–N	1.05	4.781527	0	0.009339
	Cr–(N–C)	1.19	-1.162468	0	0.00627797
	Cr–Cr	1.15	-8.087871	0	0.0018053
[6] Cr^{II}–N≡C–Cr^{III}	Cr–C	0.856501	10	0	0.002885
	Cr–N	1.140056	8.385928	0	0.029949
	Cr–(N–C)	1.199842	9.331722	0	0.009274
	Cr–Cr	1.193243	-9.938339	0	0.0020185
[7] Cr^{III}–C≡N–Cr^{II}	Cr–C	0.91093	-4.106673	0.005846	0.003193
	Cr–N	0.958863	9.996942	-0.031325	0.003707
	Cr–(C–N)	1.00967	9.999086	0	0.01525
	Cr–Cr	1.195103	-10	-0.02671	0.00203

Notes and references

1 S.-I. Ohkoshi, A. Fujishima and K. Hashimoto, *J. Am. Chem. Soc.*, 1998, **120**, 5349–5350.

2 T. Nuida, T. Hozumi, W. Kosaka, S. Sakurai, S. Ikeda, T. Matsuda, H. Tokoro, K. Hashimoto and S.-I. Ohkoshi, *Polyhedron*, 2005, **24**, 2901–2905.

3 E. Coronado, M. Makarewicz, J. P. Prieto-Ruiz, H. Prima-García and F. M. Romero, *Adv. Mater.*, 2011, **23**, 4323–4326.

4 F. J. Luque, I. A. Kowalik, J. P. Prieto-Ruiz, M. A. Niño, H. Prima-García, F. M. Romero, D. Arvanitis, E. Coronado, R. Miranda and J. J. de Miguel, *J. Mater. Chem. C*, 2018, **6**, 8171–8186.

5 E. Coronado, M. Fitta, J. P. Prieto-Ruiz, H. Prima-García, F. M. Romero and A. Cros, *J. Mater. Chem. C*, 2013, **1**, 6981–6985.

6 E. Stavitski and F. M. F. de Groot, *Micron*, 2010, **41**, 687–694.

7 `http://www.anorg.chem.uu.nl/CTM4XAS/index.html`.

8 H. Ogasawara, A. Kotani, K. Okada and B. T. Thole, *Phys. Rev. B*, 1991, **43**, 854–859.

9 H. Ogasawara, A. Kotani, R. Potze, G. A. Sawatzky and B. T. Thole, *Phys. Rev. B*, 1991, **44**, 5465–5469.

10 B. Ravel and M. Newville, *J. Synchrotron Rad.*, 2005, **12**, 537–541.

11 `http://cars9.uchicago.edu/ifeffit/BruceRavel/Horae`.